MethodsX 12 (2024) 102694

Contents lists available at ScienceDirect

MethodsX

journal homepage: www.elsevier.com/locate/methodsx

Beach surface model construction: A strategy approach with structure from motion - multi-view stereo

A.T.S. Ferreira[a,b,c,*], Carlos Henrique Grohmann[e], Maria Carolina Hernandez Ribeiro[d], Marcelo Soares Teles Santos[f], Regina Célia de Oliveira[c], Eduardo Siegle[b]

[a] *Technology in Environment and Water Resources, São Paulo State Technological College of Jahu, Jaú 17212-599, SP, Brazil*
[b] *Oceanographic Institute, University of São Paulo, São Paulo 05508-120, Brazil*
[c] *Institute of Geosciences of the State University of Campinas, Campinas 13083-855, SP, Brazil*
[d] *School of Arts, Sciences and Humanities, University of São Paulo (EACH-USP), Avenida Arlindo Béttio, 1000, Ermelino Matarazzo, 03828-000, São Paulo, Brazil*
[e] *Institute of Energy and Environment, University of São Paulo (IEE-USP), Avenida Professor Luciano Gualberto, 1289, Cidade Universitária, 05508-010, São Paulo, Brazil*
[f] *Techno-Science and Innovation Training Center, Federal University of Southern Bahia-UFSB, Itabuna Access Highway, km 39-Ferradas, Itabuna, 45613-204, Bahia, Brazil*

ARTICLE INFO

Method name:
Strategies for beach surface modeling with structure from movement - multi-view stereo

Keywords:
Structure from Motion
Photogrammetry
Beach Morphology
Beach Survey
GNSS

ABSTRACT

In contrast to traditional beach profiling methods like topographic surveys and GNSS, which pose significant challenges in terms of cost and time, this research underscores the efficiency, cost-effectiveness, and simplicity of terrestrial photogrammetry employing the Structure from Motion-Multi View Stereo (SfM-MVS) method. Notably, this approach enables the utilization of commonplace devices such as smartphones for data capture. The methodology integrates a 12-megapixel camera for image acquisition, processed through Agisoft Metashape Professional software, and validated for accuracy using ground control points (GCPs) and checkpoints (CKPs) calibrated via GNSS. Findings reveal substantial disparities in positional accuracy according to the Ground Control Points distribution. The study underscores the critical role of strategically distributing GCPs and CKPs in effectively mapping coastal areas, thus affirming the potential of SfM-MVS as a powerful and accessible tool for coastal monitoring initiatives. This research contributes significantly to advancing the efficiency and accessibility of beach profile monitoring, offering invaluable insights for researchers and practitioners in coastal management and environmental conservation efforts.

- A simplified beach profile modeling methodology is proposed.
- The method is faster and more cost-effective than traditional surveys (RTK GNSS, lidar, RPA).
- The study highlights the importance of GCP and CKP distribution in enhancing SfM-MVS accuracy for coastal mapping.

* Corresponding author.
E-mail address: anderson.ferreira46@fatec.sp.gov.br (A.T.S. Ferreira).

https://doi.org/10.1016/j.mex.2024.102694
Received 19 February 2024; Accepted 2 April 2024
Available online 3 April 2024

Specifications table

Subject area:	*Environmental Science*
More specific subject area:	*Coastal Geomorphology and Monitoring*
Name of your method:	Strategies for beach surface modeling with structure from movement - multi-view stereo
Name and reference of original method:	*N.A.*
Resource availability:	Software: *Agisoft Metashape Professional (https://www.agisoft.com/); **GNSS Data Processing:** PPP-IBGE service (https://www.ibge.gov.br), and Trimble's Survey Office software (version 5.50); **Hardware**: - Smartphone with a 12-megapixel camera (e.g., Apple Smartphone) - Gimbal stabilizer (e.g., DJI OM 5) - GNSS receivers (e.g., Spectra Precision SP60)*

Introduction and context

Classically, beach profile surface monitoring is carried through topographical surveys employing water level hoses, geometric leveling, or polygonation [1–4]. The use of kinematic spatial positioning by Global Navigation Satellite Systems (GNSS) for acquiring beach profiles remains prevalent today [5,6]. Nevertheless, the application of aerial photogrammetry using remotely piloted aircraft (RPA) or laser scanning with light detection and ranging (lidar) on land platforms or in RPAs has become increasingly widespread [7–9].

Despite their high accuracy, these techniques have several drawbacks, such as being time-consuming during fieldwork and becoming unproductive (e.g., classical methods), the lack of a robust point cloud (e.g., kinematics GNSS positioning), the risk of crashes or damages (e.g., RPA), and high costs (e.g., lidar). Considering these challenges, terrestrial photogrammetric surveying through Structure from Motion-Multi View Stereo (SfM-MVS) has attracted increasing interest in the geosciences for its ease of use and low cost, as it can be conducted with simple cameras and does not require geometric rigor in image acquisition [10,11].

Method details

SfM-MVS technique overview

SfM-MVS (Fig. 1) is a range imaging technique that reconstructs three-dimensional images from a series of photos taken by a moving sensor [10,11]. Similar to stereo vision, the Structure from Motion (SfM) algorithm identifies corresponding points in successive images, reconstructing their position in three-dimensional space as a function of camera displacement, resulting in a sparse (or coarse) point cloud; the Multi View Stereo step is tasked with refining the model and densifying the point cloud [11,12]. In geosciences, this technique has proven useful for generating digital elevation models with high spatial resolution for the "virtual" analysis of rocky outcrops, mining monitoring, and geotechnical studies, among others [10,11,13–15].

Data collection and 3D reconstruction

Fig. 2**a** shows the SfM-MVS beach surface acquisition scheme. For each beach, images were taken using a gimbal stabilizer DJI OM 5 and an Apple Smartphone equipped with a 12-megapixel camera (Fig. 2**b**), positioned at a height of 1.2 m and at an angle of ~45° to the ground. The photos were taken manually every step (or ~1 s) through a walk perpendicular to the coastline, which started from the waterline to the frontal dune (or boardwalk) and could be done inversely depending on the sunlight and its respective shadow projections. Adequate longitudinal overlap was ensured to guarantee corresponding points in the images and an imaged surface approximately 2 to 3 m wide (Fig. 2**a**).

The 3D reconstruction of beach surfaces by SfM-MVS is performed using Agisoft Metashape Professional software; geometric calibration is based on the inclusion of geodetic coordinates of targets identified in the images (GCPs and CKPs). Typically, these

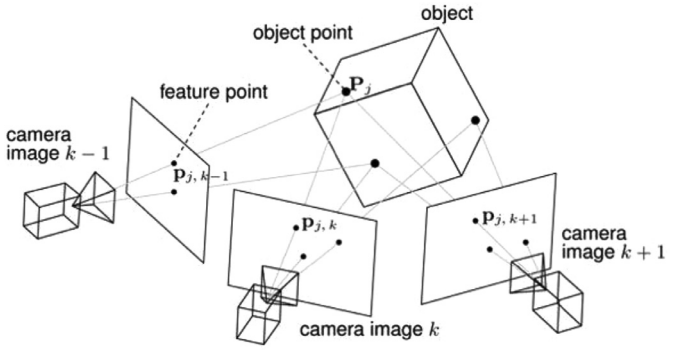

Fig. 1. Reconstitution by SfM of the projection of a point P_j of the 3D object onto the camera image at time/position k results in the tracked 2D point $p_{j,k}$ [16].

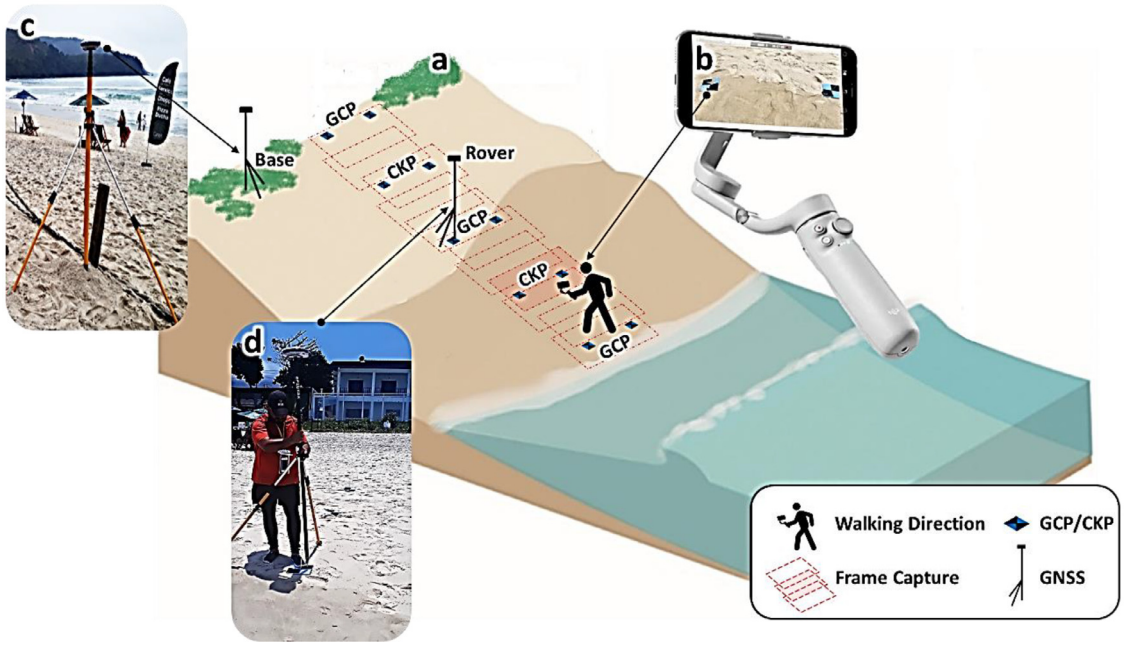

Fig. 2. (a) Beach surface acquisition scheme by SfM-MVS photogrammetric method, (b) gimbal and smartphone used to capture the surface target images (GCP and CKP), (c and d) GNSS Base and Rover.

targets are landscape objects or those implemented by the researcher (Fig. 2). The quality of the SfM-MVS models depends on the camera positioning, the quantity and distribution of GCPs and CKPs, and the camera model definition (focal length, principal point, and radial distortion) [17].

Geodetic coordinates and error analysis

The geodetic coordinates (latitude, longitude, and geometric altitude) of the GCPs and CKPs were determined by GNSS and post-processed by rapid-static relative positioning with short baselines (< 10 km), where two receivers collect data simultaneously over a time interval; one installed at a reference station ("Base", with known coordinates; Fig. 2c), and the other (Rover; Fig. 2d) at points of interest, GCPs, and CKPs [7,18].

The data tracked and stored in the Base and Rover receivers were later transferred to the computer, processed, and adjusted through the Application Programming Interface (version 1.0.0) of the *Precise Point Positioning* of the Brazilian Institute of Geography and Statistics (PPP - IBGE) and by *Trimble's Survey Office* software (version 5.50).

PPP-IBGE is a free online service for postprocessing GNSS data. This service uses the GPS Precise Point Positioning (CSRS-PPP) program developed by the Geodetic Survey Division of Natural Resources of Canada (NRCan). This allows users with GPS and GLONASS receivers to obtain precise coordinates referenced to the Geocentric Reference System for the Americas (SIRGAS2000) and the International Terrestrial Reference Frame (ITRF) [19]. The receivers used were the Spectra Precision SP60 model, which tracks observations of the phase of the carrier wave at the L1 + L2 frequency of the 6 GNSS systems (GPS, GLONASS, BeiDou, Galileo, QZSS and SBAS) and has a horizontal nominal accuracy of 3 mm + 0.5 ppm and 5 mm vertical + 0.5 ppm.

The orthometric altitudes (H_i) of the GCPs, referenced to the mean sea level of Imbituba-SC of the Brazilian Geodetic System (SBG), were calculated from the geometric altitudes (h_i) obtained by GNSS referred to the surface of the ellipsoid of revolution of the SIRGAS2000 and the geoid height (N_i) of the MAPGEO2015 model [20] (Eq. (1)):

$$H_i = h_i - N_i \tag{1}$$

Validation and application

Precision and operational simplicity test

To test and demonstrate the technique's precision, operational simplicity, and speed, different configurations between the positions of the ground control points (GCP) and check points (CKP) using SfM-MVS were examined across a single beach surface topography in Maresias, São Paulo state, Southeast Brazil (Fig. 3), which possesses all the morphological requirements needed for the proposed tests, such as varying altitudes and slopes [7]. Thus, to generate a cartographic product with relative positional accuracy on any beach profile in the shortest possible field activity time, it is essential to determine the appropriate ratio between the distribution of

Fig. 3. Location of beach surface generated by SfM-MVS, Base, and Rover GNSS with GCP and CKP locations.

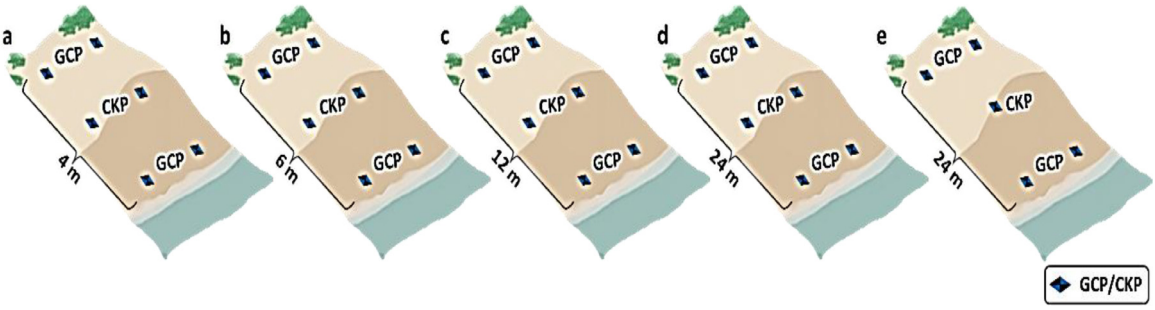

Fig. 4. Different configurations of the distribution of GCPs and CKPs along the beach profile.

materialized GCP/CKP, positioned by GNSS and identified in the images. GCPs are used to adjust the position of the images, while CKPs are employed to analyze the positional quality of the products generated [21–24].

Application and analysis

To test the best configuration of GCPs and CKPs distribution in the 3D reconstruction of beach surfaces, exploratory multivariate techniques – analytical hierarchy process-Gaussian (AHP-G) were used. The AHP-G incorporates the Gaussian distribution to quantify and assess uncertainties in evaluations and probabilistic decision-making through distributions, while retaining the classic hierarchical structure Saaty's AHP [25], without arbitrary weighting [26,27]. Thus, five configurations between GCPs and CKPs were tested along approximately 28 m of a beach profile: **a**) 4 m; **b**) 6 m; **c**) 12 m; **d**) 24 m; and **e**) 24 m. The difference between the first four configurations (profiles a-d) used two intermediate CPKs, while the last one (**e**) used only one intermediate CPK (Fig. 4).

The evaluation of the best distribution configuration between GCPs and CKPs uses normalized values of the root mean square error (RMSE; Eqs. (2) and (3)) estimates of the CKP in X, Y, Z, XY, and Total (cm). Focusing on the cost monotonic, i.e., the lower,

the better [26,27]. The result generates a ranking showing the better configuration between GCPs and CKPs.

$$RMSE = \sqrt{\sum_{i=1}^{n} \frac{\Delta H_i^2}{n}} \tag{2}$$

where $i = 1, 2, 3...n$ is the number of control points used in the evaluation, and ΔH_i is the set of discrepancies between the orthometric altitudes obtained in the model (H_i^m) and the reference altitudes (H_i^r), given by the expression:

$$\Delta H_i = H_i^m - H_i^r \tag{3}$$

Table 1 observes the five configurations (**a, b, c, d**, and **e**) and their respective accuracies of the CKP in X, Y, Z, XY, and Total (cm). Configuration "**a**" presents a higher total error, driven primarily by the error in Z. The second (**b**) has the highest total error (4.489 cm), relatively high in all categories, especially in Y and XY. The third (**c**) has a total error comparable to the first configuration (**a**), but with a significantly lower error in Y. Configuration d shows the highest error in Y and a total error slightly higher than in configurations "**a**" and "**c**". While the last (configuration "**e**") has the lowest total error, largely benefited by the lowest error in Z.

Table 2 shows the normalized error values facilitating the comparison between different configurations. In general, the values indicate that the error proportion of each column is 0.200, suggesting that, on average, the configurations equally contribute to the error in each category after normalization. Table 3 presents the standard deviation (SD), showing the dispersion of normalized errors of each configuration relative to the average. Meanwhile, the Gaussian factor (GF) considers the standard deviation, giving more weight to larger deviations, where higher values possibly indicate lower reliability. This facilitates the comparison of different configurations using the normalized Gaussian factor (NGF) [26,28].

In Table 4, the AHP-G, through NGF values, ranks the accuracies indicating configuration "**c**" (Rank 1) as the most accurate, with "**b**" being the least reliable (Rank 5). For modeling a profile in configuration (**c**), it takes about 10 s of tracking per station (GCP or CKP), with a moving speed of about 1 meter/second between each station. This totals approximately 24 s between tracking and moving between stations for every 12 m of beach profile.

Table 1
Different accuracies of the CKP (**a, b, c, d**, and **e**), respectively, in X, Y, Z, XY, and total error (cm).

Settings	X error (cm)	Y error (cm)	Z error (cm)	XY error (cm)	total error (cm)
a	1896	2135	3434	2855	4466
b	1898	2487	3219	3128	4489
c	2049	0,997	3841	2279	4466
d	1550	4071	1254	4356	4533
e	1826	3922	0,869	4326	4413

Table 2
Normalized error matrix.

Settings	X error (cm)	Y error (cm)	Z error (cm)	XY error (cm)	total error (cm)
a	0,193	0,197	0,104	0,223	0,200
b	0,193	0,169	0,111	0,204	0,199
c	0,178	0,422	0,093	0,280	0,200
d	0,236	0,103	0,284	0,146	0,197
e	0,200	0,107	0,409	0,147	0,203

Table 3
Mean, standard deviation (SD), gaussian factor (GF), and normalized gaussian factor (NGF) of the normalized errors for each configuration.

Mean	0,200	0,200	0,200	0,200	0,200
SD	0,022	0,131	0,141	0,056	0,002
GF	0,108	0,653	0,706	0,280	0,010
NGF	0,061	0,372	0,402	0,159	0,006

Table 4
Hierarchy process-gaussian (AHP-G), and Ranking.

Settings	AHP-G	Rank
a	0,164	4
b	0,153	5
c	**0,251**	**1**
d	0,191	3
e	0,241	2

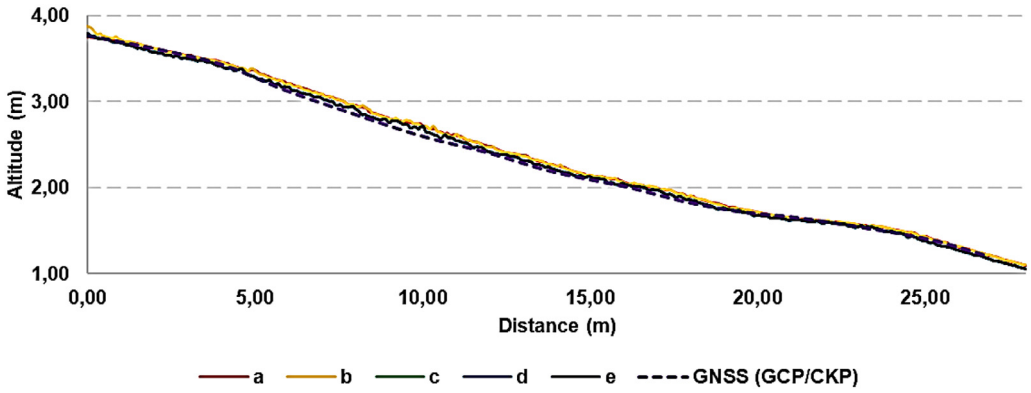

Fig. 5. Different model profiles (a, b, c, d, e, and GNSS – GCP/CKP) models along the beach profile.

In the context of error analysis, configuration '**c**' proves to be the most reliable, as reflected by its highest ranking in the Gaussian Analytic Hierarchy Process (AHP-G). This is supported by the lowest total error value compared to the other configurations, except for '**e**', which, despite having the lowest total error, received a lower ranking due to its error distribution across various dimensions. This multivariate evaluation approach is supported by Dos Dantos et al., Pereira et al., and Rodrigues et al. [26,29,30] in the AHP-G method, emphasizing the importance of considering multiple criteria in decision-making processes. Furthermore, the Gaussian adaptation employed here follows the logic presented by Buckley [31], suggesting the inclusion of probability distributions to capture the uncertainty and variability in decision-maker preferences.

Conversely, configuration '**b**', despite not presenting the highest error in any individual category, has the highest total error and, consequently, the lowest rank. This suggests that an evaluation approach based solely on aggregated errors may not adequately reflect performance in multivariate contexts. The standard deviation in the normalized matrix and the Gaussian factor play a critical role in this analysis, introducing a measure of variability that can be essential for evaluating a configuration's consistency. This notion is supported by Wong and Li [32], who highlight the relevance of standard deviation in data normalization for AHP analyses, allowing for a more robust evaluation of options. By integrating these metrics, the Gaussian AHP method provides a comprehensive and mathematically sound approach for determining the optimal configuration among multiple options with various error dimensions [26,29,30].

However, Fig. 5 reveals that the altitudinal distances between the different models generated from SfM-MVS and GNSS (GCP/CKP) appear to coincide. In this context, as the main goal of the study is to find the best way to optimize field survey time and to verify if there are significant differences between the different models, an analysis of variance was conducted to determine the presence of significant differences between the model averages, with a significance level of 95% [33,34]. Consequently, the Shapiro-Wilk test, which assesses data normality, shows p-value results lower than 0.05, indicating that the data from the evaluated models do not exhibit normality (non-parametric). Therefore, the Kruskal-Wallis test (suitable for non-parametric data sets) finds no significant difference between the model averages (p-value = 0.9171), with p-value > 0.05.

Conclusion

Thus, although the AHP-G method identifies configuration 'c' as the most accurate, the analysis of variance indicates that there is no significant difference between the models. Hence, when considering the costs involved in fieldwork, the preference usually goes to the option that minimizes time, namely, configuration "e". Thus, with just 4 GCPs and 1 CKPs positioned by GNSS and distributed every 12 m on the photographed surface, high-precision models capable of generating approximately 2 m to 3 m wide models through the SfM-MVS method can be achieved. Therefore, adding up the 30 s for tracking (5 GCPs and 1 CKP), plus the 12 s needed for image acquisition, a single person can conduct a survey in less than 1 min (~42 s) for every 12 m of beach profile. This confirms that the SfM-MVS acquisition method described in this work is suitable for various coastal applications, such as morphodynamic studies, monitoring of beach surfaces, and coastal engineering interventions.

Ethics statements

The work did not involve human beings.
The work did not involve animals.
The work did not involve data collected from social media platforms.

Declaration of competing interest

The authors declare that they have no known competing financial interests or personal relationships that could have appeared to influence the work reported in this paper.

CRediT authorship contribution statement

A.T.S. Ferreira: Conceptualization, Methodology, Software, Validation, Formal analysis, Investigation, Resources, Data curation, Writing – original draft, Writing – review & editing, Visualization, Supervision, Project administration, Funding acquisition. **Carlos Henrique Grohmann:** Methodology, Writing – original draft, Writing – review & editing, Funding acquisition. **Maria Carolina Hernandez Ribeiro:** Methodology, Investigation, Writing – original draft, Writing – review & editing. **Marcelo Soares Teles Santos:** Methodology, Formal analysis, Writing – original draft, Writing – review & editing. **Regina Célia de Oliveira:** Writing – original draft, Writing – review & editing, Visualization, Funding acquisition. **Eduardo Siegle:** Conceptualization, Methodology, Formal analysis, Investigation, Resources, Writing – original draft, Writing – review & editing, Visualization, Supervision, Project administration, Funding acquisition.

Data availability

Data will be made available on request.

Acknowledgments

The authors thank the Coastal Dynamics Laboratory of the Oceanographic Institute of the University of São Paulo, the Spatial Analysis and Modelling Lab (SPAMLab) hosted at the Institute of Energy and Environment of the University of São Paulo, the Institute of Geosciences of the State University of Campinas and the São Paulo State Technological College of Jahu, the São Paulo Research Foundation (FAPESP grant #2020/12050-6), E.S. (#308229/2022-3), C.H.G. (#311209/2021-1) and R.C.O. (#306931/2022-2) are National Council for Scientific and Technological Development (CNPq) research fellows.

References

[1] W.A. Birkemeier, A.E. DeWall, C.S. Gorbics, H.C. Miller, A User's Guide to CERC's Field Research Facility, Coastal Engineering Research Center Fort Belvoir VA, 1981.
[2] K.O. Emery, A simple method of measuring beach profiles, Limnol. Oceanogr. 6 (1961) 90–93, doi:10.4319/lo.1961.6.1.0090.
[3] D. Muehe, Geomorfologia costeira, in: S.B. Cunha, A.J.T. Guerra (Eds.), Geomorfologia: Exercícios, Técnicas e Aplicações, Editora Bertrand Brasil S.A., Rio de Janeiro, 2002, pp. 191–238.
[4] A.T. da S. Ferreira, V.E. Amaro, M.S.T. Santos, Geodésia aplicada à integração de dados topográficos e batimétricos na caracterização de superfícies de praia, Rev. Bras. Cartogr. 66 (2014) 167–184.
[5] L.P. Stein, E. Siegle, Overtopping events on seawall-backed beaches: Santos Bay, SP, Brazil, Reg. Stud. Mar. Sci. 40 (2020), doi:10.1016/j.rsma.2020.101492.
[6] A.T. da S. Ferreira, E. Siegle, M.C.H. Ribeiro, M.S.T. Santos, C.H. Grohmann, The dynamics of plastic pellets on sandy beaches: a new methodological approach, Mar. Environ. Res. 163 (2021) 105219, doi:10.1016/j.marenvres.2020.105219.
[7] J.A. Gonçalves, R. Henriques, UAV photogrammetry for topographic monitoring of coastal areas, ISPRS J. Photogramm. Remote Sens. 104 (2015) 101–111, doi:10.1016/j.isprsjprs.2015.02.009.
[8] C.H. Grohmann, G.P.B. Garcia, A.A. Affonso, R.W. Albuquerque, Dune migration and volume change from airborne LiDAR, terrestrial LiDAR and structure from motion-multi view stereo, Comput. Geosci. 143 (2020) 104569, doi:10.1016/j.cageo.2020.104569.
[9] V. Klemas, Beach Profiling, L.I.D.A.R. Bathymetry, An overview with case studies, J. Coast. Res. 27 (2011) 1019–1028, doi:10.2112/JCOASTRES-D-11-00017.1.
[10] J.L. Carrivick, M.W. Smith, D.J. Quincey, Structure from Motion in the Geosciences, John Wiley & Sons, 2016.
[11] M.J. Westoby, J. Brasington, N.F. Glasser, M.J. Hambrey, J.M. Reynolds, Structure-from-Motion'photogrammetry: a low-cost, effective tool for geoscience applications, Geomorphology 179 (2012) 300–314.
[12] F. Dellaert, S.M. Seitz, C.E. Thorpe, S. Thrun, Structure from motion without correspondence, in: Proceedings IEEE Conference on Computer Vision and Pattern Recognition. CVPR 2000 (Cat. No. PR00662), IEEE, 2000, pp. 557–564.
[13] G.P.B. Garcia, C.H. Grohmann, C.D. Viana, E.B. Gomes, Using terrestrial laser scanner and RPA-based-photogrammetry for surface analysis of a landslide: a comparison, Boletim de Ciências Geodésicas 28 (2022), doi:10.1590/s1982-21702022000300016.
[14] S. Tavani, P. Granado, A. Corradetti, M. Girundo, A. Iannace, P. Arbués, J.A. Muñoz, S. Mazzoli, Building a virtual outcrop, extracting geological information from it, and sharing the results in Google Earth via OpenPlot and Photoscan: an example from the Khaviz Anticline (Iran), Comput. Geosci. 63 (2014) 44–53, doi:10.1016/j.cageo.2013.10.013.
[15] C.D. Viana, C.H. Grohmann, M. dos Santos Toledo Busarello, G.P.B. Garcia, Structural analysis of clastic dikes using Structure from Motion - Multi-View Stereo: a case-study in the Paraná Basin, southeastern Brazil, Braz. J. Geol. 48 (2018) 839–852, doi:10.1590/2317-4889201800201898.
[16] C. Kurz, T. Thormählen, H.-P. Seidel, Visual fixation for 3D video stabilization, JVRB 8 (2011).
[17] M.R. James, S. Robson, S. d'Oleire-Oltmanns, U. Niethammer, Optimising UAV topographic surveys processed with structure-from-motion: ground control quality, quantity and bundle adjustment, Geomorphology 280 (2017) 51–66, doi:10.1016/j.geomorph.2016.11.021.
[18] J.F.G. Monico, Posicionamento Pelo GNSS: Descrição, Fundamentos e Aplicações, UNESP, São Paulo, 2008.
[19] IBGE, IBGE-PPP: Serviço On-Line Para Pós-Processamento de Dados, GNSS, Rio de Janeiro, 2020.
[20] D. Blitzkow, A.C.O.C. de Matos, E.M.L. Xavier, L.P.S. Fortes, MAPGEO2015: o novo modelo de ondulação geoidal do brasil, Rev. Bras. Cartografia (2016) 1873–1884.
[21] M.R. James, S. Robson, Mitigating systematic error in topographic models derived from UAV and ground-based image networks, Earth Surf Process. Landf. 39 (2014) 1413–1420.
[22] R.P. Lima, C. Coelho, G. Vinueza, J.T. Grassi, L.H.G. Castiglione, The use of RPAS - Remotely Piloted Aircraft Systems in the topographic mapping for mining, REM Int. Eng. J. 71 (2018) 281–287, doi:10.1590/0370-44672017710120.
[23] R.M. Gonçalves, T.F. Holanda, H.A.A. Queiroz, P.H.G.O. Sousa, P.S. Pereira, Exploring RPAS potentiality using a RGB camera to understand short term variation on sandy beaches, Catena (2022) 210, doi:10.1016/j.catena.2021.105949.
[24] R.M. Gonçalves, J.I. Pontes, F.H.M. Vasconcellos, L.A. de Alcântara Ferreira, H.A. de A. Queiroz, P.H.G. de O. Sousa, High spatial resolution data obtained by GNSS and RPAS to assess islets flood-prone scenarios for 2100, Appl. Geogr. 150 (2023) 102817, doi:10.1016/j.apgeog.2022.102817.
[25] T.L. Saaty, Decision making with the analytic hierarchy process, Int. J. Serv. Sci. 1 (2008) 83–98.
[26] M. Dos Santos, I.P. de Araújo Costa, C.F.S. Gomes, Multicriteria decision-making in the selection of warships: a new approach to the AHP method, Int. J. Anal. Hierar.Process 13 (2021).
[27] V.R. dos Santos, L.P.L. Fávero, M.Â.L. Moreira, M. dos Santos, L. de A. de Oliveira, I.P. de Araújo Costa, G.P. de Oliveira Capela, E.H. Kojima, Development of a computational tool in the Python language for the application of the AHP-Gaussian method, Procedia Comput. Sci. 221 (2023) 354–361.

[28] L. de Mattos Bento Soares, M. Santos, A. Gomes, Quadro para Tomada de Decisões estratégicas e o método AHP Gaussiano: uma abordagem multi-metodológica na seleção de um modelo de aeronave cargueira de grande porte para a Força Aérea Brasileira, 2021.
[29] R.C.A. Pereira, O.S. da Silva Jr, R.A. de Mello Bandeira, M. Dos Santos, C. de Souza Rocha Jr, C. dos S. Castillo, C.F.S. Gomes, D.A. de Moura Pereira, F.M. Muradas, Evaluation of smart sensors for subway electric motor escalators through AHP-Gaussian method, Sensors 23 (2023) 4131.
[30] M.V.G. Rodrigues, M. dos Santos, C.F.S. Gomes, Selection of helicopters for offshore service using three multi-criteria decision analysis methods: AHP-TOPSIS-2N, THOR 2 and Gaussian AHP-TOPSIS-2N, J. Control Decis. (2024) 1–15.
[31] J.J. Buckley, Fuzzy hierarchical analysis, Fuzzy Sets Syst. 17 (1985) 233–247.
[32] J.K.W. Wong, H. Li, Application of the analytic hierarchy process (AHP) in multi-criteria analysis of the selection of intelligent building systems, Build. Environ. 43 (2008) 108–125.
[33] L.P.L. Fávero, P.P. Belfiore, F.L. da Silva, B.L.P.P.-R. de J. Chan, Análise De dados: Modelagem Multivariada Para Tomada De Decisões, Elsevier, Rio de Janeiro, RJ, Brasil, 2009.
[34] L. de S. Souto, E. de S. Souto, Análise De Dados Ecológicos, 1st ed., Clude de Autores, Brasília, 2020.